KeAi
CHINESE ROOTS
GLOBAL IMPACT

Available online at www.sciencedirect.com

ScienceDirect

Advances in Climate Change Research 12 (2021) 363−372

www.keaipublishing.com/en/journals/accr/

Regional drying and wetting trends over Central Asia based on Köppen climate classification in 1961−2015

DILINUER Tuoliewubieke[a,b], YAO Jun-Qiang[a,b,*], CHEN Jing[a,b], MAO Wei-Yi[a,b], YANG Lian-Mei[a,b], YEERNAER Humaerhan[c], CHEN Yu-Hang[d]

[a] *Institute of Desert Meteorology, China Meteorological Administration, Urumqi, 830002, China*
[b] *Center of Central Asia Atmosphere Science Research, Urumqi, 830002, China*
[c] *Xinjiang Ecological Environment Monitoring Centre, Urumqi, 830011, China*
[d] *Collaborative Innovation Center on Forecast and Evaluation of Meteorological Disasters/Key Laboratory of Meteorological Disaster, Ministry of Education, Nanjing University of Information Science & Technology, Nanjing, 210044, China*

Received 20 May 2020; revised 23 November 2020; accepted 21 May 2021
Available online 1 June 2021

Abstract

Central Asia (CA) is one of the most drought-prone regions in the world with complex climate regimes, it is extremely vulnerable to water scarcity. Many studies on drought in CA, as a whole, have been carried out, whereas there is a lack of studies on the drying and wetting trends of different climatic zones within CA. In this study, CA was divided into three different climatic zones based on the Köppen climate classification method, precipitation climatology, and aridity index. These were the temperate continental (Df), dry arid desert (BW), and Mediterranean continental (Ds) climatic zones. The regional drying and wetting trends during the years 1961−2015 were investigated using the monthly gridded Standardized Precipitation Evapotranspiration Index (SPEI). The empirical orthogonal function (EOF) was applied to analyze spatial and temporal variation patterns. EOF mode 1 (EOF1) analysis found increasingly wet conditions throughout CA over the duration of the study, and EOF mode 2 (EOF2) analysis found a contrast between northern and southern CA: as Df became drier and BW and Ds became wetter. EOF mode 3 (EOF3) analysis found a western and eastern inverse phase distribution. The SPEI displayed a decreasing trend from 1961 to 1974 for CA as a whole, before increasing from 1975 to 2015, with a particularly significant increase over the first seven years of that period. On a regional scale, the BW and Ds zones experienced a wetting trend due to increased precipitation during 1961−2015, but the Df zone experienced a drying trend due to reduced evapotranspiration and an increasing temperature, particularly from 1961 to 1978. Thus, the spatio-temporal patterns in dryness and wetness across CA can be categorized according to climatic regions.

Keywords: Drought; Breaks for Additive Season and Trend (BFAST); Central Asia; SPEI; Köppen climate classification

1. Introduction

Within the context of global and regional climate change, the occurrence of frequent extreme events (e.g., rainstorms, droughts, and floods) threatens agricultural production, ecological environment, and socio-economic security and stability (Sheffield et al., 2012; Dai, 2013; Huang et al., 2016, 2017). Dry/wet variations play an important role in climate change. However, large uncertainties are associated with these changes (Dai, 2011). Therefore, a quantitative investigation of the evolution of regional dry/wet features is crucial for regional water resource management against the backdrop of a changing environment.

Central Asia (CA), one of the driest regions in the world, is located in the hinterland of Eurasia (Chen et al., 2009; Li et al., 2017). It has a complex topography consisting mainly of

* Corresponding author. Institute of Desert Meteorology, China Meteorological Administration, Urumqi, 830002, China.
E-mail addresses: yaojq1987@126.com, yaojq@idm.cn (YAO J.-Q.).
Peer review under responsibility of National Climate Center (China Meteorological Administration).

https://doi.org/10.1016/j.accre.2021.05.004

mountains, hills, plains, and deserts (Giannini et al., 2003; Chen et al., 2016). The fragile ecosystems of the area are highly sensitive and vulnerable to climate change and climate extremes (Aizen et al., 2001; Huang et al., 2013; Dai and Wang 2017; Liu et al., 2018; Guan et al., 2019). Climate change in CA has been extensively studied, revealing that the area experienced a rapid warming trend over the past century, particularly from the 1960s to 2015, with temperatures rising faster than the global mean (Lioubimtseva and Henebry, 2009; Chen et al., 2009; Chen and Huang, 2017; Yu et al., 2020). Precipitation trends are highly variable and have exhibited an increasing trend over the past century (Peng and Zhou, 2017; Hu et al., 2017; Yao et al., 2021). The frequency and intensity of extreme precipitation events over CA have increased significantly (Zhang et al., 2017; Yao et al., 2021). Climate change could accelerate the hydrological cycle, which would alter the regional dry/wet distribution.

In the past decades, the use of monitoring technology and various indices have been proposed as methods for measuring dryness and wetness, and their advantages and drawbacks have been reviewed by Zhang and Zhou (2015). Examples of meteorological drought indices include the Precipitation Anomaly (PA), Composite Index (CI), Aridity Index (AI), Palmer Drought Severity Index (PDSI), Standardized Precipitation Index (SPI), and Standardized Precipitation Evapotranspiration Index (SPEI) (Palmer, 1965; Hayes et al., 1999; McKee et al., 1993; Vicente-Serrano et al., 2010a, 2010b). Compared to other indices, the SPEI has several advantages, including its consideration of the collective influence of both precipitation and potential evaporation, flexibility of multi-time scales, and identification of more extreme events (Sun et al., 2016). Thus far, the SPEI is superior to the other indices and is widely applied in dry/wet assessment in both global and regional contexts (Zhang and Zhou, 2015; Yao et al., 2019; Wang et al., 2019).

Climate zoning was first proposed by Köppen (1884), considering air temperature, precipitation, and vegetation distribution, the method focuses on the characteristics of the overlap of climatic elements with natural geography (Köppen, 1936; Köppen and Geiger, 1954). Additionally, the Köppen climate classification has several advantages, such as clarity, fewer employed data sources, and the use of simple symbols for convenient application (Kottek et al., 2006). Based on the Köppen method, the global climate is divided into tropical, dry, warm, temperate, and polar zones and further divided into eight climatological types and 31 climatic subtypes (Peel et al., 2007). A Köppen climate classification dataset that was updated by Chen et al. (2013) is now widely used (Chen et al., 2017; Dai and Wang, 2017).

Previous studies have produced conflicting results regarding the drying and wetting trends in arid regions of CA. Some have suggested that these regions display 'dry-gets-drier' and 'wet-gets-wetter' trends, resulting in a warming-wetting trend pattern because enhanced evaporation leads to increased downward longwave radiation, specific humidity, and wetting (Held and Soden, 2006; Peng and Zhou, 2017; Hu et al., 2019; Wang et al., 2020). However, contradictory results have suggested that warming leads to an increase in aridity, as indicated by the decrease in regional precipitation observed as a possible consequence of global warming (Cook et al., 2014).

However, most of the previous studies that focused on dry and wet climates in CA were not conducted at the sub-regional scale. To illustrate the regional dry and wet features, unlike previous studies that defined the region boundary based on geography, we used the Köppen climate classification to divide CA into several climatic sub-regions to explore the relationship between climate status and dry/wet variability. Consequently, this study aims to 1) divide CA into multiple climate zones using the Köppen climate classification method, precipitation and AI climatology spatial distribution; 2) explore the characteristics of the dry and wet regional spatio-temporal patterns; 3) investigate the trends and breakpoints of the SPEI12 (the SPEI calculated at a 12-month timescale) in different regions of CA based on the Breaks for Additive Seasonal and Trend (BFAST) algorithm; and 4) delineate the relationship between the SPEI and climate factors in each time period and region. The results will provide a scientific basis for understanding, monitoring, and predicting the occurrence of drought in CA.

2. Data and method

2.1. Study area

CA is located in the center of the Eurasian continent (35°−56°N, 45°−87°E) and is far from the sea. In this study, CA encompasses five countries: Kazakhstan, Uzbekistan, Kyrgyzstan, Turkmenistan, and Tajikistan (Fig. 1). CA has diverse topography, with mountains, plains, deserts, and valleys. Due to various geomorphological and water shortages, CA has a fragile and expansive mountain−oasis−desert environment that is sensitive to dry/wet climate changes (Chen et al., 2009, 2016; Chen and Huang, 2017; Lioubimtseva and Henebry, 2009; Han et al., 2018; Zhang et al., 2019).

2.2. Data

The SPEI (Vicente-Serrano et al., 2010a, 2010b) was used as a drought index to quantify the dryness/wetness conditions in CA, which takes into account both precipitation and potential evapotranspiration based on the Penman−Monteith approach (Burke and Brown, 2006). The SPEI dataset applied was extracted from the global gridded SPEI database (v.2.5; http://spei.csic.es/database.html) with a monthly time resolution and a spatial resolution of 0.5° × 0.5°. Dryness/wetness grades were categorized as extreme drought (SPEI ≤ -2), severe drought ($-2 <$ SPEI ≤ -1.5), moderate drought ($-1.5 <$ SPEI ≤ -1), extreme wet (SPEI ≥ 2), severe wet ($1.5 \leq$ SPEI < 2), moderate wet ($1 \leq$ SPEI < 1.5), and normal state ($-1 <$ SPEI < 1). The SPEI12 was employed with the aim of studying the variability in annual dryness/wetness.

The monthly mean precipitation (PRE), potential evapotranspiration (PET), and air temperature (TMP) data were

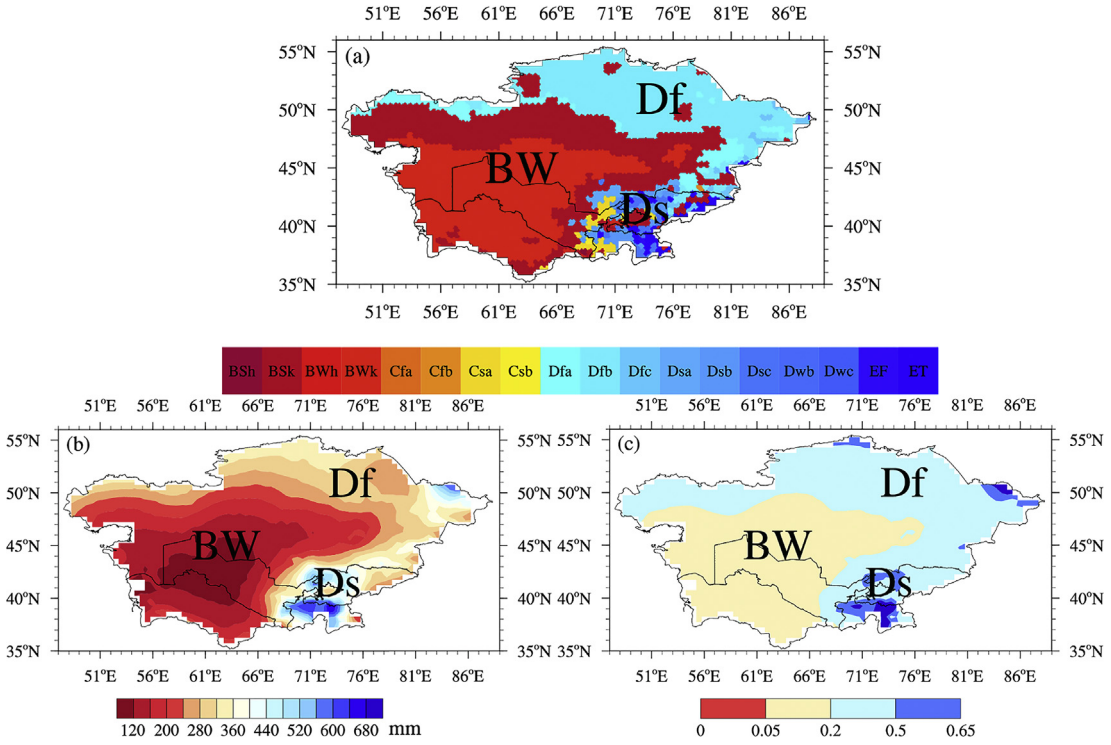

Fig. 1. Spatial distribution of (a) the three climatic zones (First letter: B, dry; C, mild temperate; D, snow; E, polar. second letter: f, fully humid; s, dry summer; w, dry winter; W, desert; s, steppe; T, tundra; F, frost. Third letter: h, hot arid; k, cold arid; a, hot summer; b, warm summer; c, cool summer), (b) long-term mean annual precipitation, and (c) aridity index over Central Asia in 1901−2010.

collected from the Climate Research Unit (CRU) Time-Series (TS) v.4.02 dataset, which has a horizontal resolution of 0.5° × 0.5° (Harris and Jones, 2019), and covers the period from 1901 to 2015. For this study, a dataset from 1961 to 2015 was extracted. Additionally, the Köppen climate classification map was employed (Chen and Chen, 2013; Chen et al., 2017) (http://hanschen.org/koppen).

2.3. Methodology

Given the high spatial variability of climatic factors in CA, it is necessary to divide climatic regions with spatial heterogeneity of climatic conditions. Therefore, the Köppen classification was employed as a diagnostic tool to monitor climatic status and divide CA into several sub-regions. This method was proposed by Chen and Chen (2013) and combines long-term global grid TMP and PRE observation datasets from several sources including the Global Historical Climatology Network 2 (GHCN2) database interpolated onto a monthly 0.5° × 0.5° grid. This was carried out for the period spanning 1901−2010 to systematically reflect the climatic conditions during this time. Fig. 1a and Table 1 describe the major climate types and climatic regions used.

The AI was adopted from the United Nations Environment Programme (UNEP) and is widely used for defining drylands; it is the most reasonable and reliable measure of climate change in drylands (UNCCD, 1994; Feng and Fu, 2013; Wang et al., 2020). The AI is defined as the ratio of annual PRE to annual PET and is a quantitative indicator of the degree of climatic dryness taking values ranging from 0.05 to 0.65 (Mortimore et al., 2009). The AI values were calculated using the PRE and PET datasets from the CRU TS v.4.02, which covers the period from 1901 to 2010. The classification criteria for the dry and wet conditions based on the AI values are listed in Table 2.

Table 1
List of climatic regions referred to in this study.

Abbreviation	Köppen climate classification	Subregion distribution
Df	Temperate continental (Dfb)	Northern Kazakhstan (48°−54°N, 61°−86°E)
BW	Dry arid desert (BWk)	Southwestern Kazakhstan, Uzbekistan, Turkmenistan (35°−48°N, 54°−68°E)
Ds	Mediterranean continental climate (Dsb)	Kyrgyzstan and Tajikistan (37°−43°N, 68°−77°E)

Table 2
Classifications of climate zones based on the annual precipitation and aridity index.

Index	Drought classification				
	Hyper-arid	Arid	Semi-arid	Dry-subhumid	Humid
Precipitation (mm)	≤50	50−200	200−400	400−600	>600
Aridity index	≤0.05	0.05−0.2	0.2−0.5	0.5−0.65	>0.65

BFAST is a change detection algorithm developed by Verbesselt et al. (2010a, 2010b) that merges the decomposition of the time series into the linear trend component (Tt), the seasonal variation component (St), and the residual component (et) to detect trends, inflection points, and the number of abrupt changes within the temporal data series. The BFAST tool was used to identify variations and trends in the monthly SPEI in CA and the defined sub-regions. The method is available in the BFAST package for R (http://cran.r-project.org/package=bfast). Readers can refer to Verbesselt et al. (2010a, 2010b) for more information.

The empirical orthogonal function (EOF) was used to extract the dominant spatial pattern according to the leading mode of the SPEI12. North statistical testing (North et al., 1982) was applied to determine the significance of the EOF modes. Linear regression was used to explore the linear trends (Sen, 1968). The Student's *t*-test (Wei, 2007) was used to examine the significance of the linear trend at the 95% confidence level.

3. Results

3.1. Climatology

Fig. 1 shows the spatial distribution of the three climatic zones: temperate continental (Dfb), dry arid desert (BWk), and Mediterranean continental (Dsb). The Dfb (hereafter referred to as Df) zone is located in northeastern Kazakhstan. The BWk (hereafter referred to as BW) zone includes parts of southwestern Kazakhstan, Uzbekistan, and Turkmenistan, including the two largest deserts, Kara-kum and Kyzyl-kum. The Dsb (hereafter referred to as Ds) zone is primarily distributed in western Kyrgyzstan and Tajikistan. These three climatic zones are affected by different atmospheric circulations. Western circulation is the primary water vapor belt supplying abundant moisture to Df regions (Aizen et al., 2001; Dai and Wang, 2017; Guan et al., 2019). The Indian monsoon influences the BW and Ds regions (Lioubimtseva and Henebry, 2009). Grasslands, deserts, and mountains are geographically distributed in the Df, BW, and Ds zones respectively.

To verify the reasonable division of the Köppen classification into three climatic patterns, the spatial distributions of precipitation and the AI climatology were compared and are given in Fig. 1b and c, respectively. Fig. 1b shows the gradual increase in the mean annual PRE from west to east over CA. Using the definition of annual PRE for drylands (Table 2), the drylands in CA are defined as having an annual PRE < 600 mm and are classified into sub-regions that are either arid (50 mm < PRE < 200 mm, BW), semi-arid (200 mm < PRE < 400 mm, Df), or dry sub-humid (400 mm < PRE < 600 mm, Ds).

Fig. 1c shows the spatial distribution of the AI. According to the AI category for distinguishing the dry/wet division, the areas that were studied belong to the drylands category (UNCCD, 1994), which are further divided into arid zones (0.05 < AI < 0.2) that are located in the BW zone in western CA; semi-arid areas (0.2 < AI < 0.65) that are further distributed in the Df zone in northern Kazakhstan; and dry sub-humid regions (or sub-humid for simplicity, 0.5 < AI < 0.65) that were found across the Ds zone in southeastern CA.

Fig. 2 shows that the combined PRE and PET displayed distinct annual cycles in both CA as a whole and in the defined sub-regions. The monthly PRE (Fig. 2a) was generally found to have two patterns of seasonal variation with a single peak or double peaks. The monthly PRE in the entire study area was large for November−January and March−May, and the monthly PRE in the Df zone had a single peak pattern with a maximum in July (39.9 mm, Fig. 2a). The Ds zone had the most abundant PRE, averaging 451.4 mm in 1961−2015. The mean annual PRE in BW areas was 160.8 mm. The monthly area-averaged PET presented unimodal patterns with a maximum in July (Fig. 2b). CA as a whole generally exhibited strong PET and sparse PRE, which is consistent with the findings of Li et al. (2015). However, each climatic type had distinct features, with significant PRE concentrations over the Df zone in the warm season and over the BW and Ds zones in the cold season. Strong PET occurred in summer over all regions. Seasonal changes in the PRE and PET levels also provide a basis for climate zoning.

3.2. Spatial characteristics of dryness and wetness

The ratio of grids at different grades of dryness and wetness during 1961−2015 are presented as histograms (Fig. 3). The results indicate that dryness and wetness have a staggered appearance in CA, with drought intensity increasing rapidly during 1970−1980 and 1995−2001. The most severe drought emerged in 1975, affecting 60.9% of CA. Among these areas, 3.4%, 18.9%, and 44.6% experienced extreme, severe, and moderate droughts, respectively (Fig. 3a). In the same year, the drought proportions in the Df, BW, and Ds zones were 59.8%, 63.4%, and 41.9%, respectively, suggesting that the drought occurred in 1975. The year with severe dry conditions was also consistent with findings of Hu et al. (2019) who reported the years of major drought. In 1996, the highest probability of drought occurrence reached 41.6%. Drought in the BW zone accounted for 70.5% of the total occurrence. The years in which more than 40% of the grids in CA featured different grades of wetness were 1964 (51.7%), 1993 (41.4%), 2002 (49.8%), and 2003 (46.7%). Moderate and high droughts were observed in the northern Df regions during 1974−1978, 1994−2000, and 2005−2012, with proportions reaching values of 59.1% and 56.7% in 1975 and 1998, respectively (Fig. 3b). In the BW zone consisting of desert regions (Fig. 3c), large variability was observed in the intensity of wetness and dryness; consecutive droughts occurred during 1975−1977 and 1995−2001, and wet periods occurred during 1966−1970, 1978−1984, 1987−1994, 2002−2005, and 2012−2015. The intensity of drought in mountainous areas of the Ds zone (Fig. 3d) was relatively low, and wet events were more common in 1969, with wetness ratios exceeding 40%. Furthermore, 2002−2006 and 2009−2015 were particularly wet periods.

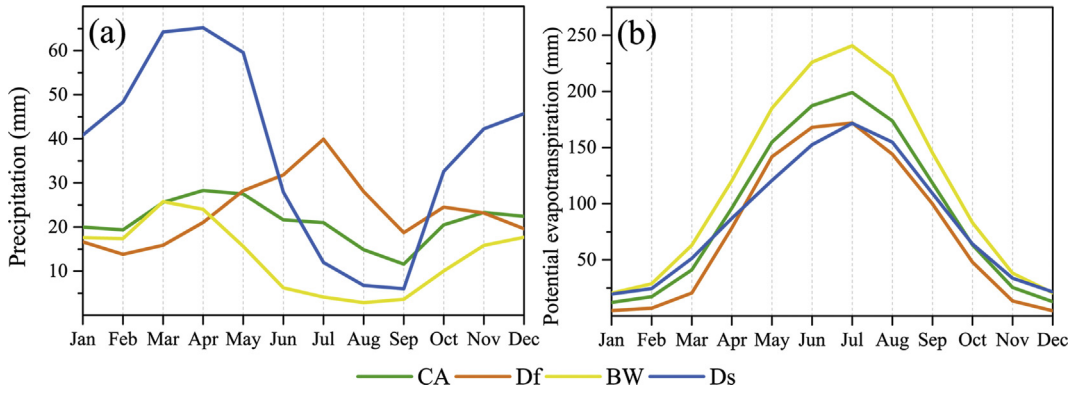

Fig. 2. Annual cycles of precipitation (a) and potential evapotranspiration (b) in Central Asia and the three sub-regions of Df, BW, and Ds during 1961−2015.

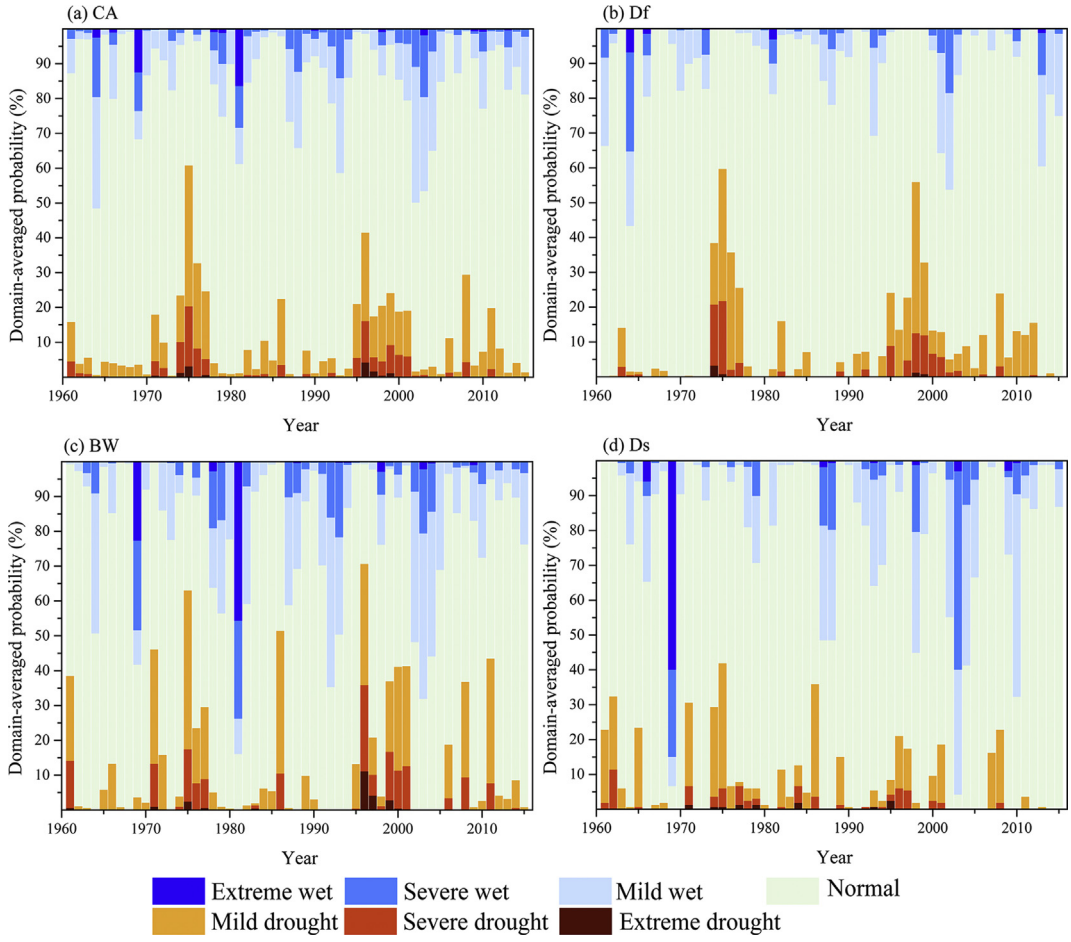

Fig. 3. Ratio of grids for different grades of dryness/wetness from 1961 to 2015 in the whole Central Asia and three sub-regions.

To explore the dominant spatio-temporal distribution of dry and wet variability over CA during 1961−2015, the derived EOF modes of the SPEI are shown in Fig. 4. The first three leading EOF modes account for 44.9% of the total variance, and pass the North test rule (North et al., 1982).

The first EOF mode of variability for the SPEI explained 23.1% of the total variance (Fig. 4a1), which is characterized by uniform variations with maximum positive loadings. Minimum positive loadings were distributed in the Df zone. The corresponding time series exhibited decadal fluctuations (Fig. 4a2), indicating fluctuations in dry-wet-dry-wet transitions. The EOF2 describes 13.6% of the total variance, which has a dipole-like pattern with reverse-loading signs over the northern and southern parts of CA (Fig. 4b1). PC2 was characterized by alternating dryness and wetness periods (Fig. 4b2). EOF3 shows a dipole pattern with the largest

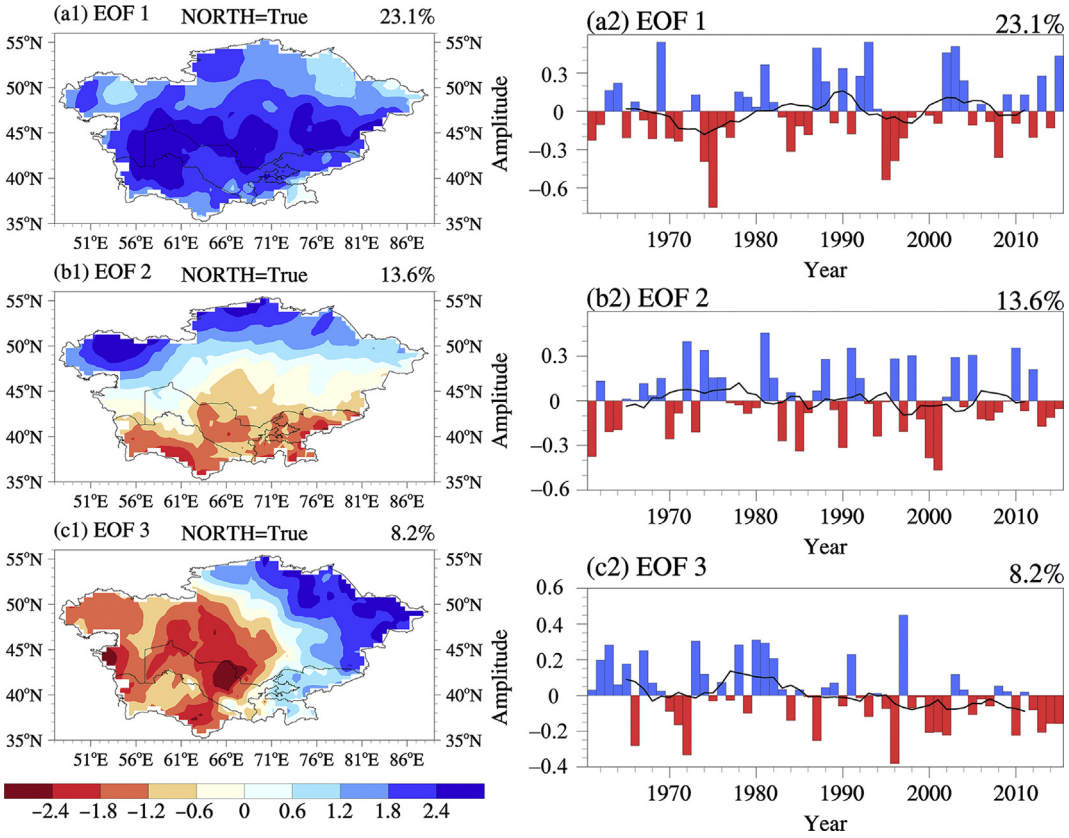

Fig. 4. Spatial pattern (a1, b1, c1) and corresponding principal component (a2, b2, c2) of the first three EOF models of SPEI12 during 1961−2015 (Note that the EOF spatial pattern (time series) is multiplied (divided) by 100. NORTH = True indicates that EOFs were significant based on the North test).

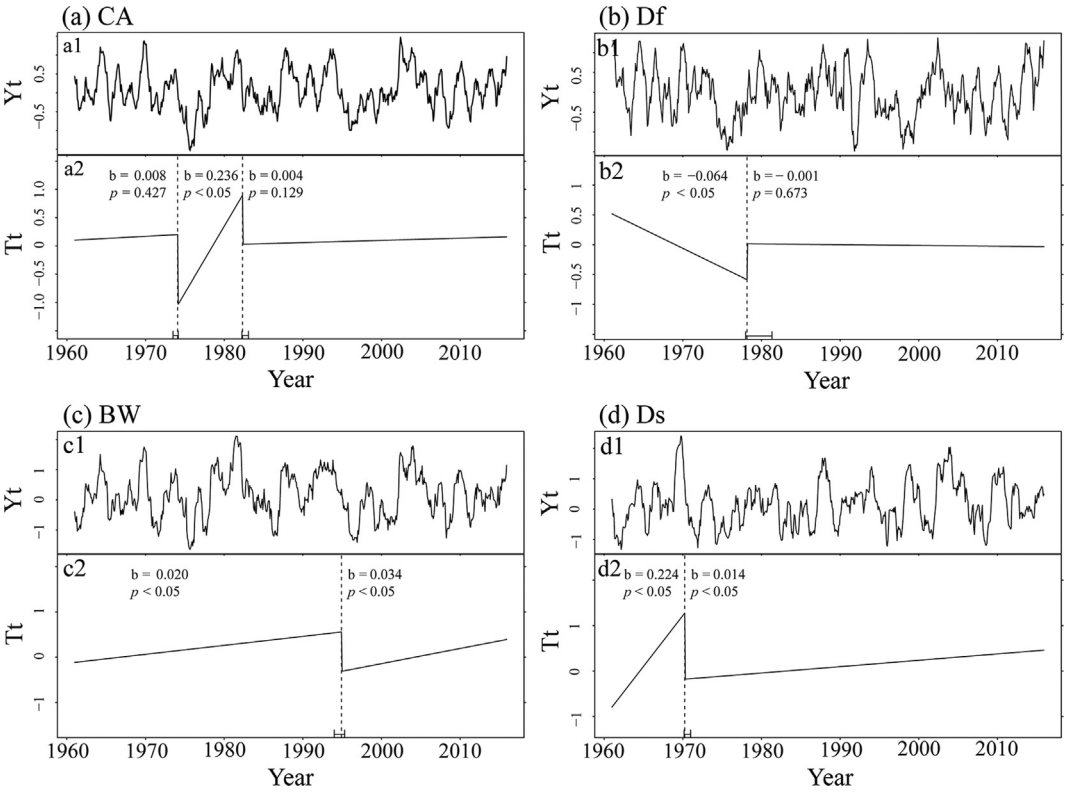

Fig. 5. Detected changes of monthly gridded SPEI time series by BFAST for Central Asia and sub-regions from January 1961 to December 2015 (a1, b1, c1, and d1 represent the time series (Yt) of the monthly SPEI, while a2, b2, c2, and d2 represent variation trends (Tt)).

loading primarily located in the east and the smallest in the west (Fig. 4c1).

3.3. Drying and wetting trends over CA

Breakpoints were found within the trend component over CA as a whole and over the three sub-regions, as shown in Fig. 5. Breakpoints occurred in September 1974 and March 1982. Decrease-increase-increase (D−II−I type) trends were detected across the entire study period and indicated a very rapid increase in wetness period after the first breakpoint. During 1975−1982, the amplitude of the trend in the regional SPEI was 0.29 mm per year ($p < 0.05$), which suggests that during this interval, conditions in CA tended towards wetness.

The BFAST method was used to decompose the SPEI value over each sub-region (Fig. 5b−d), and it was found that there was one significant breakpoint within the long-term time series. The breakpoint occurred in 1978 for the Df zone, in 1994 for the BW zone, and in 1970 for the Ds zone. Overall, the SPEI did not continuously increase or decrease for the entire study region or individual sub-regions.

3.4. Relationship between SPEI, PET, PRE, and TMP

To elucidate the effect of climatic driving factors on the SPEI in CA and the three sub-regions during 1961−2015, the partial correlation coefficient was calculated to quantify the impact of PET, PRE, and TMP on the SPEI changes (Table 3). A decrease in PET or an increase in PRE and TMP increased the SPEI for CA as a whole and for the Ds zone. An increase in PRE or decrease in PET and TMP resulted in an increased SPEI for the Df and BW zones. PRE was found to play an important role in dry/wet conditions, showing the highest positive correlation coefficient. PET featured a significant negative correlation and mean temperature had the smallest effect on the SPEI.

To better understand the likely mechanisms driving changes in SPEI, it is necessary to investigate the variation of climatic driving factors (PET, PRE, and TMP) and its magnitude during different time periods and regions.

Across the entire CA, all climatic factors showed negative trends during the first segment period from 1961 to 1974

Table 3
Partial correlation coefficient between the annual SPEI and climatic driving factors (annual PET, annual PRE, and annual TMP) over the entire CA region and sub-regions during 1961−2015.

Study area	PET	PRE	TMP
CA	−0.53*	0.78*	0.02
Df	−0.59*	0.74*	−0.02
BW	−0.53*	0.86*	−0.07
Ds	−0.57*	0.81*	0.07

Note: * $p < 0.01$.

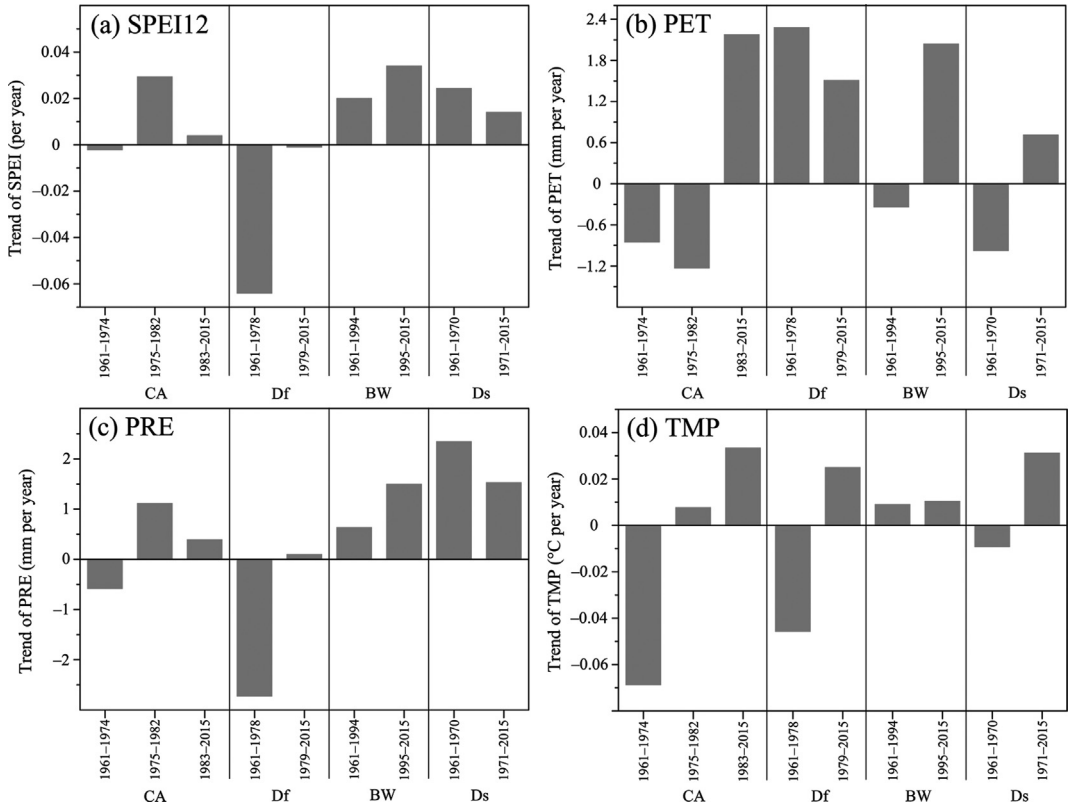

Fig. 6. Trend of the annual mean SPEI (a) and climate factors (b, PET; c, PRE; d, TMP) for CA or each climatic sub-region during segmented time periods based on the breakpoints.

(Fig. 6). While PET exhibited a negative trend, PRE and TMP displayed positive trends during the second period 1975−1982. During the final period, the SPEI12 and all three climate factors showed increasing trends (Fig. 6). It was found that across CA, PET decreases and PRE increases were associated with increases in the SPEI. The SPEI for the Df zone decreased from drastic to slight (DD−D type) during this period (Fig. 6a). This suggests that PET had the largest positive increase, accompanied by a decrease in PRE during the first period, which was the dominant factor for decreasing the SPEI. Trends in the SPEI in the BW and Ds zones were positive for each time period (Fig. 6a), PET decreased during the first period, increased during the second period, while PRE decreased for both the BW and Ds zones.

4. Conclusions and discussion

CA based on the Köppen climate classification, precipitation climatology, and the aridity index, the CA was divided into three sub-regions: temperate continental (Df), dry arid desert (BW), and Mediterranean continental (Ds) climatic zones. The SPEI displayed a decreasing trend during 1961−1974 for the whole CA region, before increasing from 1975 to 2015. On a regional scale, the BW and Ds zones displayed wetting trends due to increased precipitation during 1961−2015, but the Df zone showed drying trends due to reduced potential evapotranspiration and increasing temperature, especially in the period of 1961−1978.

Previous studies have reported that warmer conditions lead to increased aridity (Cook et al., 2014), and that the 'dry-gets-drier' and 'wet-gets-wetter' pattern has been recognized across the globe owing to the warming climate (Held and Soden, 2006; Chou et al., 2013). However, different patterns were observed in the different regions studied. In CA, Chou et al. (2013) confirmed that the dryness and wetness levels indicate a warmer or drier climate as a result of PRE decrease. However, Peng et al. (2017) and Hu et al. (2019) reported that CA has recently become warmer and wetter. We divided CA into three sub-regions based on climatic classification methods and found that CA as a whole region experienced a trend toward wetter conditions. The Df zone of the westerly regime (Dai and Wang, 2017) became dryer, while the BW and Ds zones of the Mediterranean-type regions became wetter. Thus, the spatio-temporal pattern in the changes in dryness/wetness in CA can be categorized by considering the link between climatic regions and regional climatic status.

The SPEI is based on the monthly climatic water balance and shows different sensitivities to PRE and PET. Vicente-Serrano et al. (2015) suggested that the SPEI is most sensitive to PET variability. Sun et al. (2016) also highlighted the importance of PET in determining dry/wet conditions in the southeastern region of CA. Peng and Zhou (2017) pointed out that the increased PET in the arid areas of Northwestern China caused increased downward longwave radiation, contributing to the dominant specific humidity. However, we found that PRE plays an important and positive role in the climate of CA and each of the three climatic sub-regions studied. Each of sub-region was also impacted by PET. In the arid desert area (BW), increased PRE caused humidification but could not reverse the desert conditions. This study considers only three meteorological factors, but the drought and wetness variations in CA and the sub-regions are also influenced by PET components, such as sunshine duration and wind speed. Abnormal atmospheric circulation also greatly influences dry/wet conditions (Lioubimtseva and Henebry, 2009). Additionally, human activities, vegetation coverage, groundwater level, and soil moisture all contribute to controlling regional drought and wetness. Thus, future studies should consider the effects of atmospheric circulation and human activity on drought conditions in CA (Zhu et al., 2020).

Declaration of competing interest

The authors declare no conflict of interest.

Acknowledgments

This research was funded by National Key Research and Development Program of China (2018YFC1507101), National Natural Science Foundation of China (U1903113), China Desert Meteorological Science Research Foundation (SQJ2017012), and Sichuan Science and Technology Program (2020JDJQ0050).

The CRU data obtained from the Centre for Environmental Data Analysis (http://data.ceda.ac.uk/badc/cru/data/cru_ts4.02). The monthly gridded SPEI data was available from the digital CSICS (http://spei.csic.es/database.html). The ASCII file of the Köppen climate classification data was available at http://hanschen.org/Köppen.

References

Aizen, E., Aizen, V., Melack, J.M., et al., 2001. Precipitation and atmospheric circulation patterns at mid-latitudes of Asia. Int. J. Climatol. 21, 535−556. https://doi.org/10.1002/joc.626.

Burke, E.J., Brown, S.J., Christidis, N., 2006. Modeling the recent evolution of global drought and projections for the twenty-first century with the Hadley Centre Climate Model. J. Hydrometeorol. 7 (5), 1113−1125. https://doi.org/10.1175/jhm544.1.

Chen, D.L., Chen, H.W., 2013. Using the Köppen classification to quantify climate variation and change: an example for 1901−2010. Environ. Develop. 6, 69−79. https://doi.org/10.1016/j.envdev.2013.03.007.

Chen, F.H., Huang, W., 2017. Multi-scale climate variations in the arid Central Asia. Adv. Clim. Change Res. 8, 1−2. https://doi.org/10.1016/j.accre.2017.02.002.

Chen, F.H., Wang, J.S., Jin, L.Y., et al., 2009. Rapid warming in min-latitude central Asia for the past 100 years. Front. Earth Sci. China 3 (1), 42−50. https://doi.org/10.1007/s11707-009-0013-9.

Chen, T., Zhang, H., Chen, X., et al., 2017. Robust drying and wetting trends found in regions over China based on Köppen climate classifications. J. Geophys. Res. Atmos. 122 (8), 4228−4237. https://doi.org/10.1002/2016JD026168.

Chen, Y.N., Li, W.H., Deng, H.J., et al., 2016. Changes on Central Asia's water tower: past, present and future. Sci. Rep. 6, 35458. https://doi.org/10.1038/srep35458.

Chou, C., Chang, J., Lan, C., et al., 2013. Increase in the range between wet and dry season precipitation. Nat. Geosci. 6, 263−267. https://doi.org/10.1038/ngeo1744.

Cook, B., Smerdon, J., Seager, R., et al., 2014. Global warming and 21st century drying. Clim. Dynam. 43, 2607−2627. https://doi.org/10.1007/s00382-014-2075-y.

Dai, A., 2011. Drought under global warming: a review. Wiley Interdiscip. Rev. Clim. Change 2, 45−65. https://doi.org/10.1002/wcc.81.

Dai, A., 2013. Increasing drought under global warming in observations and models. Nat. Clim. Change 3, 52−58. https://doi.org/10.1038/nclimate1633.

Dai, X.G., Wang, P., 2017. A new classification of large-scale climate regimes around the Tibetan Plateau based on seasonal circulation patterns. Adv. Clim. Change Res. 8 (1), 26−36. https://doi.org/10.1016/j.accre.2017.01.001.

Feng, S., Fu, Q., 2013. Expansion of global drylands under a warming climate. Atmos. Chem. Phys. 13 (19), 10081−10094. https://doi.org/10.5194/acp-13-10081-2013.

Giannini, A., Saravanan, R., Chang, P., 2003. Oceanic forcing of Sahel rainfall on interannual to interdecadal time scales. Science 302, 1027−1030. https://doi.org/10.1126/science.1089357.

Guan, X.F., Yang, L.M., Zhang, Y.X., et al., 2019. Spatial distribution, temporal variation, and transport characteristics of atmospheric water vapor over Central Asia and the arid region of China. Global Planet. Change 172, 159−178. https://doi.org/10.1016/j.gloplacha.2018.06.007.

Han, Q.F., Li, C.F., Zhao, C.Y., 2018. Grazing decreased water use efficiency in Central Asia from 1979 to 2011. Ecol. Model. 388, 72−79. https://doi.org/10.1016/j.ecolmodel.2018.09.020.

Harris, I.C., Jones, P.D., 2019. CRU TS4.02: climatic research unit (CRU) time−series (TS) version 4.02 of high-resolution gridded data of month-by-month variation in climate (Jan. 1901−Dec. 2017). Centre for Environmental Data Analysis. https://doi.org/10.5285/b2f81914257c4188b181a4d8b0a46bff.

Hayes, M.J., Svoboda, M.D., Wilhite, D.A., et al., 1999. Monitoring the 1996 drought using the standardized precipitation index. Bull. Am. Meteorol. Soc. 80, 429−438. https://doi.org/10.1175/1520-0477(1999)080<0429:MTDUTS>2.0.CO;2.

Held, I.M., Soden, B.J., 2006. Robust response of the hydrological cycle to global warming. J. Clim. 19 (21), 5686−5699. https://doi.org/10.1175/JCLI3990.1.

Huang, J.P., Yu, H., Guan, X., et al., 2016. Accelerated dryland expansion under climate change. Nat. Clim. Change 6 (2), 166−172. https://doi.org/10.1038/nclimate2837.

Huang, J.P., Li, Y., Fu, C., et al., 2017. Dryland climate change: recent progress and challenges. Rev. Geophys. 55, 719−778. https://doi.org/10.1002/2016RG000550.

Huang, W., Chen, F.H., Feng, S., et al., 2013. Interannual precipitation variations in the mid-latitude Asia and their association with large scale atmospheric circulation. Chin. Sci. Bull. 58 (32), 3962−3968. https://doi.org/10.1007/s11434-013-5970-4.

Hu, Z.Y., Zhou, Q., Chen, X., et al., 2017. Variations and changes of annual precipitation in Central Asia over the last century. Int. J. Climatol. 37, 157−170. https://doi.org/10.1002/joc.4988.

Hu, Z.Y., Chen, X., Chen, D.L., et al., 2019. "Dry gets drier, wet gets wetter": a case study over the arid regions of Central Asia. Int. J. Climatol. 39, 1072−1091. https://doi.org/10.1002/joc.5863.

Kottek, M., Grieser, J., Beck, C., et al., 2006. World Map of the Köppen-Geiger climate classification updated. Meteorol. Z. 15 (3), 259−263. https://doi.org/10.1127/0941-2948/2006/0130.

Köppen, W., 1884. The thermal zones of the Earth according to the duration of hot, moderate and cold periods and of the impact of heat on the organic world (translated and edited by Volken, E., and Brönnimann, S.). Meteorol. Z. 20, 351−360.

Köppen, W., 1936. Das Geographische System der Klimate. Gebrüder Borntraeger, Berlin.

Köppen, W., Geiger, R., 1954. Klima der Erde (climate of the earth). Wall map 1:16 mill. Klett-Perthes, Gotha.

Li, Z., Chen, Y.N., Li, W.H., et al., 2015. Potential impacts of climate change on vegetation dynanics in Central Asia. J. Geophys. Res. 120, 12345−12356 https://doi.org/10.1002-2015JD023618.

Li, Z., Chen, Y.N., Fang, G.H., et al., 2017. Multivariate assessment and attribution of droughts in Central Asia. Sci. Rep. 7, 1316. https://doi.org/10.1038/s41598-017-01473-1.

Lioubimtseva, E., Henebry, G.M., 2009. Climate and environmental change in arid Central Asia: impacts, vulnerability, and adaptations. J. Arid Environ. 73 (11), 963−977. https://doi.org/10.1016/j.jaridenv.2009.04.022.

Liu, Y., Wu, C., Jia, R., et al., 2018. An overview of the influence of atmospheric circulation on the climate in arid and semi-arid region of Central and East Asia. Sci. China Earth Sci. 61, 1183−1194. https://doi.org/10.1007/s11430-017-9202-1.

McKee, T.B., Doesken, N.J., Kleist, J., 1993. The relationship of drought frequency and duration to timescales. Eighth Conference on Applied Climatology. Calif, pp. 179−186.

Mortimore, M., Anderson, S., Cotula, L., et al., 2009. Dryland opportunities: a new paradigm for people, ecosystems and development. IUCN, Gland.

North, G.R., Bell, T.L., Cahalan, R.F., et al., 1982. Sampling errors in the estimation of empirical orthogonal functions. Mon. Weather Rev. 110 (7), 699−706.

Palmer, W.C., 1965. Meteorological drought research paper 45. U.S. Department of Commerce Weather Bureau, Washington DC.

Peel, M.C., Finlayson, B.L., McMahon, T.A., 2007. Updated world map of the Köppen-Geiger climate classification. Hydrol. Earth Syst. Sci. 11, 1633−1644.

Peng, D.D., Zhou, T.J., 2017. Why was the arid and semiarid northwest China getting wetter in the recent decadal? J. Geophys. Res. Atmos. 122, 9060−9075. https://doi.org/10.1002/2016JD026424.

Sen, P.K., 1968. Estimates of the regression coefficient based on Kendall's tau. J. Am. Stat. Assoc. 63 (324), 1379−1389. https://doi.org/10.1080/01621459.1968.10480934.

Sheffield, J., Wood, E.F., Roderick, M.L., 2012. Little change in global drought over the past 60 years. Nature 491, 435−438. https://doi.org/10.1038/nature11575.

Sun, S.L., Chen, H.S., Wang, G.J., et al., 2016. Shift in potential evapotranspiration and its implications for dryness/wetness over Southwest China. J. Geophys. Res. 121, 9342−9355. https://doi.org/10.1002/2016JD025276.

UN (United Nations), 1994. United Nations convention to combat desertification. Geneva, Switzerland.

Verbesselt, J., Hyndman, R., Newnham, G., et al., 2010a. Detecting trend and seasonal changes in satellite image time series. Rem. Sens. Environ. 114 (1), 106−115. https://doi.org/10.1016/j.rse.2009.08.014.

Verbesselt, J., Hyndman, R., Zeileis, A., et al., 2010b. Phenological change detection while accounting for abrupt and gradual trends in satellite image time series. Rem. Sens. Environ. 114 (12), 2970−2980. https://doi.org/10.1016/j.rse.2010.08.003.

Vicente-Serrano, S.M., Beguería, S., López-Moreno, J.I., 2010a. A multiscalar drought index sensitive to global warming: the standardized precipitation evapotranspiration index. J. Clim. 23 (7), 1696−1718. https://doi.org/10.1175/2009jcli2909.1.

Vicente-Serrano, S.M., Beguería, S., López-Moreno, J.I., et al., 2010b. A global 0.5° gridded dataset (1901−2006) of a multiscalar drought index considering the joint effects of precipitation and temperature. J. Hydrometeorol. 11 (4), 1033−1043. https://doi.org/10.1175/2010JHM1224.1.

Vicente-Serrano, S.M., Schrier, G.V.d., Beguería, S., 2015. Contribution of precipitation and reference evapotranspiration to drought indices under different climates. J Hydrol 526, 42−54. https://doi.org/10.1016/j.jhydrol.2014.11.025.

Wang, Q., Zhai, P.M., Qin, D.H., 2020. New perspectives on 'warming−wetting' trend in Xinjiang, China. Adv. Clim. Change Res. 11 (3), 252−260. https://doi.org/10.1016/j.accre.2020.09.004.

Wang, Y.F., Liu, G.X., Guo, E.L., 2019. Spatial distribution and temporal variation of drought in inner Mongolia during 1901-2014 using standardized precipitation evapotranspiration index. Sci. Total Environ. 654, 850−862. https://doi.org/10.1016/j.scitotenv.2018.10.425.

Wei, F.Y., 2007. Modern Climatic Statistical Diagno-Sis and Prediction Technology, second ed. China Meteorological Press, Beijing (Chinese).

Yao, J.Q., Tuoliewubieke, D., Chen, J., et al., 2019. Identification of drought events and correlations with large-scale ocean-atmospheric patterns of variability: a case study in Xinjiang, China. Atmosphere 10 (2), 94. https://doi.org/10.3390/atmos10020094.

Yao, J.Q., Chen, J., Zhang, T.W., et al., 2021. Stationarity in the variability of arid precipitation: a case study of arid Central Asia. Adv. Clim. Change Res. 12 (2), 172−186. https://doi.org/10.1016/j.accre.2021.03.013.

Yu, Y., Chen, X., Markus, D., et al., 2020. Climate change in Central Asia: sino-German cooperative research findings. Sci. Bull. 65, 689−692. https://doi.org/10.1016/j.scib.2020.02.008.

Zhang, J., Chen, H.S., Zhang, Q., 2019. Extreme drought in the recent two decades in northern China resulting from Eurasian warming. Clim. Dynam. 52, 2885−2902. https://doi.org/10.1007/s00382-018-4312-2.

Zhang, L.X., Zhou, T.J., 2015. Drought over East Asia: a review. J. Clim. 28 (8), 3375−3399. https://doi.org/10.1175/JCLI-D-14-00259.1.

Zhang, M., Chen, Y., Shen, Y., et al., 2017. Changes of precipitation extremes in arid Central Asia. Quat. Int. 436, 16−27. https://doi.org/10.1016/j.quaint.2016.12.024.

Zhu, X., Wei, Z.G., Dong, W.J., et al., 2020. Dynamical downscaling simulation and projection for mean and extreme temperature and precipitation over central Asia. Clim. Dynam. 54, 3279−3306. https://doi.org/10.1007/s00382-020-05170-0.